isvr Institute of Sound and Vibration Research

Combining the Active Control of Gear Vibration with Condition Monitoring

M.H. Chen and M.J. Brennan

ISVR Technical Memorandum 824

December 1997

University of Southampton

SCIENTIFIC PUBLICATIONS BY THE ISVR

Technical Reports are published to promote timely dissemination of research results by ISVR personnel. This medium permits more detailed presentation than is usually acceptable for scientific journals. Responsibility for both the content and any opinions expressed rests entirely with the author(s).

Technical Memoranda are produced to enable the early or preliminary release of information by ISVR personnel where such release is deemed to the appropriate. Information contained in these memoranda may be incomplete, or form part of a continuing programme; this should be borne in mind when using or quoting from these documents.

Contract Reports are produced to record the results of scientific work carried out for sponsors, under contract. The ISVR treats these reports as confidential to sponsors and does not make them available for general circulation. Individual sponsors may, however, authorize subsequent release of the material.

UNIVERSITY OF SOUTHAMPTON

INSTITUTE OF SOUND AND VIBRATION RESEARCH

STRUCTURAL DYNAMICS GROUP

Combining the Active Control of Gear Vibration with Condition Monitoring

by

M.H. Chen and M.J. Brennan

ISVR Technical Memorandum No. 824

December 1997

Abstract

In this report, an established gear meshing model is first used to derive the secondary force required to cancel the gear vibration with actuators positioned on the gear itself. The ratio of the secondary force to the contact force between meshing teeth is found to be the stiffness modulation index of the gear meshing stiffness. Equations to determine the required forces for the specially configured actuators and the actual accelerations in three directions from three sensors on the gear are derived. The difficulty in measuring the stiffness variation function and the characteristics of the magnetostrictive actuators call for an adaptive controller to be integrated into the active control system. An adaptive harmonic controller is adopted because it is most suitable to control the vibration generated by meshing teeth due to the nature of gear vibration. It is found that the gear vibration generated by the stiffness variation can be suppressed by the specially configured actuators, leaving the vibration caused defects intact. Two time-frequency distributions are used to analyse the vibration signals and it is shown that the higher order moment spectra gives better results in detecting faults on gear teeth. Some previous proposed stiffness variation functions are found to be inappropriate for the study reported here. Other researchers have suggested that the decrease in meshing stiffness is the source of vibration generated by meshing gears with faults on teeth faces. However, the results obtained from simulations in this report suggest that that the discontinuity of the first derivative in the stiffness variation function results in the gear vibration generated by faults on teeth.

Contents

Notation

a	maximum variation ratio of the meshing stiffness
a_n	coefficients of the Fourier series of the compliance function
b	a constant
c	damping in the linear oscillator
c'	equivalent viscous damping coefficient
$d(t)$	disturbance
$e[\theta(\tau)]$	spatially periodic displacement excitation function in the linear oscillator
$e'[\theta(t)]$	spatially periodic displacement excitation function
$f = F/k_0E$	dimensionless mean load
$f_a[\theta(\tau)]$	dimensionless time-varying load
f_n	forces generated by actuators (n=1,2,3)
Δf	amplitude of a dimensionless time-varying load
$k[\theta(\tau)] = k_0 + k_a[\theta(\tau)]$	spatially periodic stiffness function in the linear oscillator
$k'[\theta(t)]$	spatially periodic stiffness function
$k_0 = \langle k \rangle_\theta$	time-invariant component of the stiffness k
$k_a[\theta(t)]$	spatically periodic alternating component of the stiffness k
m	mass of the linear oscillator
m_e	equivalent mass of meshing gears
r	distance of actuators to the centre O
r_n	pitch circle radius of gears (n=0, 1, 2)
$s(t)$	an analytical signal
Δ_s	amplitude of a dimensionless displacement
$u(t)$	output of the frequency-domain controller
v	quadrature amplitude of the frequency-domain controller output
w	in-phase amplitude of the frequency-domain controller output
x	relative displacement of meshing teeth
x_0	maximmum deviation from the designed relative displacement
$y(t)$	output of the parametric excitation system

$\mathbf{A}$	coefficients matrix
E	unit displacement
$\mathbf{F}$	force matrix
F	a constant load in the linear oscillator model
$F'(x,\theta)$	parametric excitation term
F_0	a constant force
$\Delta F[\theta(t)]$	a time-varying load in the linear oscillator model
I_n	polar moment of inertia of gears (n=1,2)
J	cost function
J_a	approximated cost function
K	constant stiffness
N	an integer
O	centre of the gear
P	force between meshing teeth along the path of contact
P_0	equivalent contact force of T_n (n=1,2) along the path of contact
$\overline{P}_0$	mean value of P_0
$\Delta P_0(\theta)$	variation of P_0 with respect to $\overline{P}_0$
$\Delta P_0' = \sigma \cdot \Delta P_0$	a time-varying load
$\mathbf{R}$	distance matrix
R	local autocorrelation
S	spectral density of s
T_n	constant torques on shafts (n=1,2)
T'	torques caused by friction
W_s	Wigner-Ville distribution of the signal s
W_s^n	WHOMS of order n of the signal s
α	stiffness modulation index
α_n	coefficients (n=0,1,2,...)
$\beta = bE$	dimensionless angle modulation depth
β_n	coefficients (n=0,1,2,...)
$\delta = e(\theta)/E$	dimensionless displacement excitation function

$\varepsilon(t)$	measured periodic error
$\zeta = c/2\sqrt{k_0 m}$	damping ratio
θ	angular displacement
$\theta(\tau) = \Lambda\tau + \beta\xi(\tau)$	angular parameter
θ_0	initial angular displacement
μ	convergence coefficient
$\xi(\tau) = x(\tau)/E$	dismesionless displacement coordinate
$\hat{\xi}$	quasi-static loaded excitation function
$\sigma = \sum_{n=1}^{2} \frac{r_n^2}{I_n}$	a constant
$\tau = \omega_n t$	dimensionless time variable
	time lag
τ_d	time delay
ϕ	pressure angle
ϕ_n	angular displacement of gears (n=1,2)
ϕ_s	phase angle
$\alpha\psi[\theta(\tau)] = k_a[\theta(\tau)]/k_0$	dimensionless variation of stiffness
ω	frequency
$\omega_n = \sqrt{k_0/m}$	static natural frequency of the linear oscillator system
$\Theta = \omega t + \theta_0$	angular displacement
Ω	time-invariant mean angular velocity
$\Lambda = \Omega/\omega_n$	dimensionless frequency ratio

1. Introduction

This technical discusses the combination of the active control of gear vibration with condition monitoring. Specially configured actuators and sensors make it possible to control the gear vibration at the source and minimise the effects of transmission paths on measured vibration signals. The sensors used for the active control system can also be used to acquire the signals for the purpose of condition monitoring of gear meshing.

The report is concerned with (1) a gear meshing model with secondary forces applied, (2) the active control of gearing vibration using three specially configured secondary actuators, (3) the adaptive controller for the attenuation of gearing vibration, and (4) the condition monitoring of gearing vibration, using Wigner-Ville distribution (WVD) and Wigner Higher Order Moment Spectra (WHOMS).

A simple gear model without applied secondary forces has been proposed by Chen & Brennan [1] to analyse the dynamics of a pair of meshing gears. This has been further simplified to a linear oscillator similar to the one discussed by Blankenship & Singh [2]. In this report, a model of meshing gears with secondary forces is first established, followed by the requirements and effects of secondary forces for vibration cancellation.

The method proposed to suppress the gearing vibration preserves the spirit of noise and vibration control - "Control at the source". It is shown that the force ratio of the secondary force required for complete cancellation of gearing vibration to meshing forces is only dependent on the index of meshing stiffness variation. This together with the meshing force determines the type of actuators which should be used for the purpose of vibration control.

The difficulty in measuring the variation of teeth meshing stiffness and the nonlinearity of magnetostrictive actuators demands an adaptive controller to be integrated into the active vibration control system. An adaptive harmonic controller proposed by Sutton & Elliott [3] is capable of suppressing harmonic disturbances in nonlinear systems. The adaptive controller used in this report is studied in the frequency domain which is suitable for the attenuation of gearing

vibration since the frequencies of vibration generated by meshing teeth are all related to the rotational speed of shafts (shaft order) on which gears are mounted.

Two time-frequency distributions, Wigner-Ville distribution (WVD) [4,5] and Wigner Higher Order Moment Spectra (WHOMS) [6,7,8], are employed to diagnose the conditions of meshing gears by monitoring the vibration signals. WHOMS preserves the properties of WVD and extends them to the higher-order spectra domain. Results of both methods are compared to show their differences and advantages.

In the following sections this report sets out the modelling of meshing gears with applied secondary forces and goes on to describe specially configured actuators which will be implemented in future experiments to provide the required secondary forces. This is followed by a discussion of the adaptive controller used for the attenuation of harmonic disturbances and time-frequency methods for the condition monitoring of meshing gears. Finally, simulation results are presented to show the limitations of the gear meshing model described and the capability of the adaptive feedforward control scheme.

2. Gear meshing model and the determination of secondary forces

The model of meshing gears proposed in [1] is further extended in this section to investigate the feasibility incorporating a secondary force onto the gear to cancel the gear vibration generated by teeth meshing.

2.1 Gear meshing model

The dynamics of one pair of meshing gears is schematically shown in figure (2.1). Assuming torques T_1 and T_2 in figure (2.1) are functions of θ, i.e. $T_1(\theta)$ and $T_2(\theta)$, the equation of motion for the driving gear can be written as:

$$T_1 - Pr_1\cos\phi - T_1' = I_1\ddot{\phi}_1 \tag{2.1}$$

and for the driven gear:

$$Pr_2\cos\phi + T_2' - T_2 = I_2\ddot{\phi}_2 \tag{2.2}$$

In equations (2.1) and (2.2), $T_1(\theta)$ and $T_2(\theta)$ can be represented by the product of a force $\left(P_0 = \overline{P}_0 + \Delta P_0(\theta)\right)$ along the path of contact and the gear radius $\left(T_1 = P_0 r_1\cos\phi,\ T_2 = P_0 r_2\cos\phi\right)$. Hence, equations (2.1) and (2.2) become:

$$\ddot{\phi}_1 = -\left(P - \overline{P}_0 - \Delta P_0(\theta)\right)\frac{r_1\cos\phi}{I_1} - \frac{T_1'}{I_1} \tag{2.3}$$

$$\ddot{\phi}_2 = \left(P - \overline{P}_0 - \Delta P_0(\theta)\right)\frac{r_2\cos\phi}{I_2} + \frac{T_2'}{I_2} \tag{2.4}$$

The relative displacement, x, between the driving and the driven gear wheels is given by $x = r_1\phi_1 - r_2\phi_2$, so that equations (2.3) and (2.4) combine to give:

$$\ddot{x} = -\left(P - \Delta P_0(\theta)\right)\left(\frac{r_1^2}{I_1} + \frac{r_2^2}{I_2}\right)\cos\phi - \left(\frac{T_1' r_1}{I_1} + \frac{T_2' r_2}{I_2}\right) + \overline{P}_0\left(\frac{r_1^2}{I_1} + \frac{r_2^2}{I_2}\right)\cos\phi \tag{2.5}$$

Equation (2.5) can be written as:

$$\ddot{x} + c'\dot{x} + F'(x,\theta) = F_0 \tag{2.6}$$

in which, $c'\dot{x} = \left(\frac{T_1' r_1}{I_1} + \frac{T_2' r_2}{I_2}\right)$, $F'(x,\theta) = (P - \Delta P_0(\theta))\left(\frac{r_1^2}{I_1} + \frac{r_2^2}{I_2}\right)\cos\phi$, and $F_0 = \overline{P}_0\left(\frac{r_1^2}{I_1} + \frac{r_2^2}{I_2}\right)\cos\phi$.

The contact force between meshing teeth can be expressed as [9]:

$$P(x,\theta) = K(1 + a\cos\theta)(x - x_0\cos\theta)_+ \tag{2.7}$$

Substituting equation (2.7) into equation (2.6), gives:

$$\ddot{x} + c'\dot{x} + \sigma K(1 + a\cos\theta)x - \Delta P_0(\theta)\sigma = \sigma F_0 + \sigma K(1 + a\cos\theta)(x_0\cos\theta) \tag{2.8}$$

where $\sigma = \left(\frac{r_1^2}{I_1} + \frac{r_2^2}{I_2}\right)$.

Setting a spatially periodic stiffness function $k'[\theta(t)] = k'[\theta(t) + 2\pi] = K(1 + a\cos\theta)$, and a spatially periodic displacement excitation function then equation (2.8) can be further written as:

$$\ddot{x} + c'\dot{x} + \sigma k'[\theta(t)]x(t) = \sigma F_0 + \sigma\Delta P_0 + \sigma k'[\theta(t)]e'[\theta(t)] \tag{2.9}$$

Dividing equation (2.9) by the constant σ, here an equivalent mass m which can be represented by $m = 1/\sigma = m_1 m_2/2(m_1 + m_2)$ is used. Equation (2.9) can be schematically realised by a linear oscillator shown in figure (2) by introducing the relative displacement between meshing teeth which simplifies the two DOF (degree of freedom) gear meshing model to a single DOF linear system, and can be written as:

$$m\ddot{x} + c\dot{x} + k[\theta(t)]x(t) = F + \Delta F[\theta(t)] + k[\theta(t)]e[\theta(t)] \tag{2.10}$$

where $m\ddot{x}$ is the inertial force, $c\dot{x}$ is the damping force, $k[\theta(t)]x(t)$ results from the variation of stiffness, F is a constant load, ΔF is a time-varying load, and $k[\theta(t)]e[\theta(t)]$ is due to the displacement excitation. The physical system for equation (2.10) is shown in figure (2.2).

The mass m shown in equation (2.10) is the equivalent mass for meshing gears in the rotational model, and other coefficiente are all scaled by this equivalent coefficient.

2.2 Liner oscillator

In order to investigate the interactions between the mean force, displacement excitation and stiffness, equation (2.10) can be further written as [1,2]:

$$\ddot{\xi}+2\zeta\dot{\xi}+\{1+\alpha\psi[\theta(\tau)]\}\xi(\tau)=f+f_a[\theta(\tau)]+\{1+\alpha\psi[\theta(\tau)]\}\delta[\theta(\tau)] \tag{2.11}$$

in which, the dots denotes differentiation with respect to τ. Validations of this parametric equation for gear vibration can also be found in [10]. Only three simple harmonic forms of the dimensionless stiffness variation $\psi(N\theta)$, the dimensionless displacement excitation function $\delta(\theta)$ and the dimensionless time-varying load $f_a(N\theta)$ are considered in this report:

$$\psi(\theta)=\cos(N\theta) \tag{2.12}$$

$$\delta(\theta)=\Delta_s\cos(\theta+\phi_s) \tag{2.13}$$

$$f_a(N\theta)=\Delta f\cos(N\theta) \tag{2.14}$$

Equation (2.11) can also be written in terms of an equivalent quasi-static loaded excitation function $\hat{\xi}(f,\theta)$ [2]:

$$\ddot{\xi}+2\zeta\dot{\xi}+\{1+\alpha\psi[\theta(\tau)]\}\xi(\tau)=\{1+\alpha\psi[\theta(\tau)]\}\hat{\xi}[f,\theta(\tau)] \tag{2.15}$$

where $\hat{\xi}(f,\theta)$ may be computed or measured under quasi-static conditions as $\Lambda\to 0$ ($\dot{\xi}=0$ and $\ddot{\xi}=0$) and can be derived from equation (2.11) [2]:

$$\hat{\xi}(f,\theta)=\delta(\theta)+(f+f_a(\theta))/[1+\alpha\psi(\theta)] \tag{2.16}$$

This compliance function (can be found in [1]) is an even function which is periodic in $N\theta$ and can be expressed in terms of the Fourier coefficients:

$$[1+\alpha\cos(N\theta)]^{-1}=\sum_{n=0}^{\infty}a_n\cos(nN\theta) \tag{2.17}$$

in which, n is the mesh harmonic index and a_n is given by:

$$a_0 = \frac{1}{\sqrt{1-\alpha^2}} \qquad n=0, \qquad a_n = \frac{2}{\sqrt{1-\alpha^2}}\left(\frac{\sqrt{1-\alpha^2}-1}{\alpha}\right)^n \qquad n=1,2,3... \quad (2.18)$$

To gain insight into the effects of the mean load, stiffness variation, and the time-varying load on the generation of higher order mesh harmonics, the stiffness term in equation (2.15) is replaced by its spatially averaged mean value, a linear differential equation with time-invariant (LTI) coefficients can be obtained:

$$\ddot{\xi} + 2\zeta\dot{\xi} + \xi(\tau) = \hat{\xi}[f, \theta(\tau)] \qquad (2.19)$$

The linear differential equation (2.19) approximates the parametric equation (2.15) by neglecting the consideration of instability which can be found in [1]. Nevertheless, it is found that the linear differential equation can be used to predict the gear vibration satisfactorily.

2.3 Determination of secondary forces

In this section, efferts are made to determine the secondary forces required for the actuators positioned on the gear to cancel the gear vibration.

Equation (2.19) together with equations (2.13), (2.14), (2.15), (2.16) and (2.17) becomes:

$$\ddot{\xi}(\tau) + 2\zeta\dot{\xi}(\tau) + \xi(\tau) = \Delta_s \cos(\Lambda\tau + \phi_s) + f \cdot \sum_{n=0}^{\infty} \cos(nN\Lambda\tau) + \Delta f \sum_{n=0}^{\infty} \cos(nN\Lambda\tau)\cos(N\Lambda\tau) \qquad (2.19a)$$

The steady state solution of equation (2.19a) can be written as [see Appendix A for a detailed derivation]:

$$\begin{aligned} \xi_{ss}(\tau) = {} & \frac{\Delta_s\left[\left(1-\Lambda^2\right)\cos(\Lambda\tau+\phi_s) + (2\zeta\Lambda)\sin(\Lambda\tau+\phi_s)\right]}{\left(1-\Lambda^2\right)^2 + (2\zeta\Lambda)^2} \\ & + f \cdot \sum_{n=0}^{\infty} \frac{a_n\left\{\left[1-(nN\Lambda)^2\right]\cos(nN\Lambda\tau) + 2\zeta(nN\Lambda)\sin(nN\Lambda\tau)\right\}}{\left[1-(nN\Lambda)^2\right]^2 + \left[2\zeta(nN\Lambda)\right]^2} \\ & + \Delta f \cdot a_0 \frac{\left\{\left[1-(N\Lambda)^2\right]\cos(N\Lambda\tau) + 2\zeta(N\Lambda)\sin(N\Lambda\tau)\right\}}{\left[1-(N\Lambda)^2\right]^2 + \left[2\zeta(N\Lambda)\right]^2} \end{aligned} \qquad (2.20)$$

$$+\Delta f \cdot \sum_{n=1}^{\infty} \frac{a_n}{2} \frac{\left\{\left[1-((n+1)N\Lambda)^2\right]\cos((n+1)N\Lambda\tau)+2\zeta((n+1)N\Lambda)\sin((n+1)N\Lambda\tau)\right\}}{\left[1-((n+1)N\Lambda)^2\right]^2+\left[2\zeta((n+1)N\Lambda)\right]^2}$$

$$+\Delta f \cdot \sum_{n=1}^{\infty} \frac{a_n}{2} \frac{\left\{\left[1-((n-1)N\Lambda)^2\right]\cos((n-1)N\Lambda\tau)+2\zeta((n-1)N\Lambda)\sin((n-1)N\Lambda\tau)\right\}}{\left[1-((n-1)N\Lambda)^2\right]^2+\left[2\zeta((n-1)N\Lambda)\right]^2}$$

Assuming $\Delta_s = 0$, i.e. no dimensionless displacement excitation, in equation (2.10), and collecting terms, equation (2.20) can be further written as:

$$\xi_{ss}(\tau) = \sum_{n=0}^{\infty} C_n \frac{\left\{\left[1-(nN\Lambda)^2\right]\cos(nN\Lambda\tau)+\left[2\zeta(nN\Lambda)\right]\sin(nN\Lambda\tau)\right\}}{\left[1-(nN\Lambda)^2\right]^2+\left[2\zeta(nN\Lambda)\right]^2} \tag{2.20a}$$

Coefficients of each frequency in equation (2.20a) can be written as:

$(0*N\Lambda)$ $$C_0 = a_0 f + \frac{a_1}{2}\Delta f \tag{2.21a}$$

$(1*N\Lambda)$ $$C_1 = a_1 f + \left(a_0 + \frac{a_2}{2}\right)\Delta f \tag{2.21b}$$

$(2*N\Lambda)$ $$C_2 = a_2 f + \left(\frac{a_1}{2} + \frac{a_3}{2}\right)\Delta f \tag{2.21c}$$

$(3*N\Lambda)$ $$C_3 = a_3 f + \left(\frac{a_2}{2} + \frac{a_4}{2}\right)\Delta f \tag{2.21d}$$

$\vdots$

Setting equation (2.21b) to zero, the force ratio can be obtained:

$$\frac{\Delta f}{f} = \frac{-2a_1}{2a_0 + a_2} = \alpha \tag{2.22}$$

Substituting equation (2.22) into equations (2.21a,c,d), the coefficient of $(0*N\Lambda)$ term is f, and coefficients of other frequencies are all zero. Results shown in figure (2.3) are obtained by substituting equation (2.22) into equation (2.11) with three different secondary forces, 25% Δf, 50% Δf and 100% Δf, respectively. The force df shown in figure (2.3) is the force Δf used in this section.

It can be seen that for $\Delta f = \alpha \cdot f$, the peak-to-peak amplitude is zero everywhere except for $N\Lambda = 2$ which is caused by the instability and the amplitude is determined by the damping in the system. The secondary force required to fully cancel the gearing vibration can be determined using equation (2.22).

The result obtained in equation (2.22) shows that the force ratio between the secondary forces required for actuators positioned on the gear to cancel gear vibration and the teeth contact force is the stiffness modulation index α. At the first sight, this may restrict the applications of this proposed control scheme for the active control of gear vibration, it is found that for higher ccontact ratio meshing gears, the stiffness modulation index can be small, and the contact force between meshing teeth is dependent on the linear speed at the contact point and the transmitted power of meshing teeth which may still make this control scheme applicable.

3. Actuator configuration

Section 2 showed that in principle that gear vibration can be controlled using secondary forces on meshing gears. In this section, efforts are made to investigate the feasibility of placing actuators on one of meshing gears to cancel the gearing vibration. Secondary forces generated by three actuators on a rotating disk are considered in this section.

3.1 Configuration

Three actuators are required to balance the force acting at the central position (O in figure (3.1)) and the torque caused by the applied force P_0, which is a function of time, i.e. there will not be any extra forces caused by three actuators except the cancellation of resultant forces in the x-, y-directions and torque at centre O caused by the fluctuating force P_0. These three actuators are positioned $2\pi/3$ radians apart as shown in figure (3.1). The forces exerted on the disc are labelled as f_1, f_2, and f_3, and all are in the tangential directions. The distance between the actuators and the centre O is denoted by r. Force P_0 acts at the edge of this disc (radius r_0) along the line contact with the pressure angle ϕ with respect to the tangential direction.

3.2 Equilibrium equations

The force P_0 shown in figure (3.1) contains only the fluctuating terms which together with the constant component (not considered in figure (3.1)) causes the variations of applied force and torque at centre O. The objectives of actuators are to cancel the fluctuating forces (both in the x & y directions) and the fluctuating torque generated by the external force P_0. Hence, in the x-direction, the equation of equilibrium can be written as:

$$f_1 \sin(\omega t + \theta_0) + f_2 \sin(\omega t + \theta_0 - 2\pi/3) + f_3 \sin(\omega t + \theta_0 - 4\pi/3) = -P_0 \sin\phi \qquad (3.1)$$

and the equilibrium equation in the y-direction is given by:

$$f_1 \cos(\omega t + \theta_0) + f_2 \cos(\omega t + \theta_0 - 2\pi/3) + f_3 \cos(\omega t + \theta_0 - 4\pi/3) = -P_0 \cos\phi \qquad (3.2)$$

and the third equation is for the balance of the torque about centre O:

$$f_1 r + f_2 r + f_3 r = -P_0 r_0 \cos\phi \qquad (3.3)$$

Combining equations (3.1-3.3), they can be written in a matrix form:

$$\mathbf{A}(\omega, t, \theta_0)\cdot\mathbf{F} = -P_0\mathbf{R} \tag{3.4}$$

where

$$\mathbf{A} = \begin{bmatrix} \sin(\omega t+\theta_0) & \sin(\omega t+\theta_0-2\pi/3) & \sin(\omega t+\theta_0-4\pi/3) \\ \cos(\omega t+\theta_0) & \cos(\omega t+\theta_0-2\pi/3) & \cos(\omega t+\theta_0-4\pi/3) \\ r & r & r \end{bmatrix} \tag{3.5}$$

$$\mathbf{F}=[f_1\ f_2\ f_3]^T \tag{3.6}$$

$$\mathbf{R} = \left[\sin\phi \quad \cos\phi \quad r_0\cos\phi\right]^T \tag{3.7}$$

The force on each actuator can be obtained from equation (3.4), and can be written as:

$$\mathbf{F} = -P_0\mathbf{A}^{-1}\mathbf{R} \tag{3.8}$$

Each force is expressed as follow:

$$f_1 = \frac{-P_0}{3r}\left\{2r\sin\phi\sin\Theta + 2r\cos\phi\cos\Theta + r_0\cos\phi\right\} \tag{3.9}$$

$$f_2 = \frac{-P_0}{3r}\left\{-r\sin\phi\left[\sin\Theta+\sqrt{3}\cos\Theta\right] + r\cos\phi\left[\sqrt{3}\sin\Theta-\cos\Theta\right] + r_0\cos\phi\right\} \tag{3.10}$$

$$f_3 = \frac{-P_0}{3r}\left\{r\sin\phi\left[-\sin\Theta+\sqrt{3}\cos\Theta\right] - r\cos\phi\left[\sqrt{3}\sin\Theta+\cos\Theta\right] + r_0\cos\phi\right\} \tag{3.11}$$

where $\Theta = \omega t + \theta_0$. The maximum ratio of force of one actuator to the external force P_0 can be determined from equation (3.9), by differentiating it with respect to time t and setting it to zero. The maximum ratio is found to be:

$$\left|f_1/|P_0\right\|_{max} = \frac{1}{3}\left(2+\frac{r_0}{r}\cos\phi\right) \tag{3.12}$$

It can be seen that the maximum ratio is frequency independent. Since these three actuators are symmetrically positioned, the maximum force ratio for each actuator is equivalent, they only differ in phase lag (i.e. time delay).

Results shown in figure (3.2) are obtained by setting $\theta_0 = 0$, $\omega = 1$, $\phi = 20^\circ$, r=0.1 m, r_0=0.15 m, and $P_0 = 100\cos(2\pi \cdot 16t)$. The forces obtained for actuators in this case can be treated as the forces required to cancel the gear vibration for a gear with 16 teeth, and the force shown is for one revolution of the gear.

4. Adaptive harmonic controller

The nonlinearity of actuators, the progression of faults on gear teeth, and the characteristics of gearing vibration call for a frequency-domain adaptive controller. The block diagram of this adaptive harmonic controller is shown in figure (4.1) which is similar to the one proposed by Sutton and Elliott [3].

Referring to equations (2.14) and (2.22), the secondary force required to completely cancel the gearing vibration is a single tone sinusoidal wave whose amplitude is decided by the index of stiffness variation of meshing gears. First, a linear actuator is assumed which can be easily extended to handle multi input multi output systems.

The in-phase and quadrature amplitudes, w_1 and v_1, of the frequency domain controller output u(t) are adapted by using the gradient descent algorithm. The cost function J to be minimised is chosen to be the mean squared error averaged over one rotation of the gear which actuators are mounted on.

$$J = \frac{1}{T}\int_{-T/2}^{T/2} \varepsilon^2(t)dt \tag{4.1}$$

where $\varepsilon(t)$ is the measured periodic error, i.e. the torsional acceleration determined by accelerations measured by three accelerometers placed on the gear, which is the sum of the disturbance d(t) and the output y(t) of the parametric excitation system. If the error $\varepsilon(t)$ is written as:

$$\varepsilon(t) = \sum_{n=1}^{\infty}\left[\alpha_n \cos(nN\omega t) + \beta_n \sin(nN\omega t)\right] \tag{4.2}$$

Then the cost function can be approximated, only the first harmonic is considered, and by Parseval's theorem, written as:

$$J_a = \frac{1}{2}\left(\alpha_1^2 + \beta_1^2\right) \tag{4.3}$$

The controller output u(t) is:

$$u(t) = w_l \cos(N\omega t) + v_l \sin(N\omega t) \tag{4.4}$$

The gradient descent algorithm to update the controller coefficients w_l and v_l at the i-th period is:

$$w_l(i+1) = w_l(i) - \mu \frac{\partial J_a}{\partial w_l(i)} \tag{4.5a}$$

$$v_l(i+1) = v_l(i) - \mu \frac{\partial J_a}{\partial v_l(i)} \tag{4.5b}$$

There are two parameters, $\partial J_a/\partial w_l$ and $\partial J_a/\partial v_l$, in equation (4.5) to be determined from the actual system before adopting the adaptive algorithm. Nevertheless, simulations results shown in this report are carried out in the linear region, the coefficients (w_l, v_l) of controller can be found directly from the spectral density of the error signal.

The advantages using this frequency domain adaptive harmonic controller are

(1) The nonlinearity of actuators can be taken into consideration.

(2) No attention has to be paid to the causality problems of the controller since the coefficients w_n and v_n can be adapted to cope with the time delay caused by the error path.

5. Condition monitoring: time-frequency distribution

The Wigner-Ville distribution has been a well-known time-frequency distribution to engineers. The recently developed WHOMS is based on the WVD and comparisons of these two distributions are given in this section.

Two time-frequency distributions, the Wigner-Ville distribution (WVD) [4,5] and the sliced Wigner Higher Order Moment Spectra (WHOMS) [6,7,8] are used in this report to monitor the conditions of meshing gears in which the localised defects generate non-stationary signals. WVD and WHOMS have some similar properties in terms of the correlation of input signals. Introductions to these two distributions are given as follow:

5.1 Wigner-Ville distribution

The WVD can be derived from the relationship between the autocorrelation function and the power spectrum for non-stationary, time-variant signals, which represents the instantaneous power spectral density. The WVD is defined as [4]

$$W_s(t,\omega) = \int_{-\infty}^{+\infty} s^*\left(t-\frac{\tau}{2}\right)s\left(t+\frac{\tau}{2}\right)e^{-j\omega\tau}d\tau \tag{5.1}$$

or can be defined in terms of spectrum as:

$$W_s(\omega,t) = \int_{-\infty}^{+\infty} S^*\left(\omega-\frac{\theta}{2}\right)S\left(\omega+\frac{\theta}{2}\right)e^{-j2\pi\theta t}d\theta \tag{5.2}$$

The s(t) in equation (5.1) is an analytical signal which can be obtained by using the Hilbert transform. Since the spectrum of an analytical signal does not have any negative frequencies, it prevents the interference between positive and negative frequencies [5].

In practical applications, it is often that only a limited length of data is available. The pseudo WVD is defined by employing a windowing function $h(\tau)$ into the integral in equation (5.1).

$$W_s^p(t,\omega) = \int_{-T/2}^{T/2} h(\tau)s^*\left(t-\frac{\tau}{2}\right)s\left(t+\frac{\tau}{2}\right)e^{-j\omega\tau}d\tau \tag{5.3}$$

The bilinear character of WVD leads to interference or "cross-terms" in the time-frequency domain which can be seen from the WVD over some regions without any signals existing. The interference can be removed by using Choi-Williams distribution [11] at the expense of losing resolution. Nevertheless, this property does not inhibit its application and acceptance.

5.2 Wigner higer order moment spectra

The WHOMS is illustrated here to compare its performance with WVD. The WHOMS of order n of a complex deterministic signal s(t) is defined as [6]

$$W_s^n(t,\omega_1,\ldots,\omega_n) = \int_{\tau_1}\ldots\int_{\tau_n} R_s^n(t,\tau_1,\ldots,\tau_n)\prod_{i=1}^{n} e^{-j\omega_i\tau_i} d\tau_i \tag{5.4}$$

where

$$R_s^n(t,\tau_1,\ldots,\tau_n) = s^*(t-\tau_d)\prod_{i=1}^{n} s^{(*)^{i+1}}(t+\tau_i-\tau_d) \tag{5.5}$$

The notation $(*)^{i+1}$ used in equation (5.5) denotes conjugation if (i+1) is odd, and no conjugation if (i+1) is even. The time delay τ_d should be properly chosen to satisfy the three basic properties of time-frequency distribution [7] , namely (a) shift in time (or frequency) of the signal should result in a corresponding shift of the distribution, (b) the integral of the distribution over all frequencies (or time) should be equal to the instantaneous power (or spectral density), and (c) the mean frequency (or time) of the distribution at each time (frequency) should be equal to the instantaneous frequency (or group delay), and is found:

$$\tau_d = \frac{1}{n+1}\sum_{i=1}^{n}\tau_i \tag{5.6}$$

The symmetric Wigner trispectrum can be written as [8]

$$W_s^3(t,\omega_1,\omega_2,\omega_3) = \iiint s^*(t-\tau)s(t-\tau+\tau_1)s^*(t-\tau+\tau_2)s(t-\tau+\tau_3)e^{-j(\omega_1\tau_1+\omega_2\tau_2+\omega_3\tau_3)}d\tau_1 d\tau_2 d\tau_3 \tag{5.7}$$

where

$$\tau = \frac{\tau_1+\tau_2+\tau_3}{4} \tag{5.8}$$

By setting $\omega_1 = -\omega_2 = \omega_3 = \omega$, the sliced Wigner trispectrum (SWT) is obtained which significantly reduces the number of cross terms [8] and the SWT is used in this report. A more detail descriptions of SWT can be found in [8].

6. Simulation

The variation of gear meshing stiffness is considered to be the most effective source of gear vibration by Dalpiaz and Meneghetti [12]. They also proposed a simple stiffness function which consists of two half-sinusoids of different amplitudes and duration superimposed on a constant term. However, this approximation of the actual meshing stiffness is found inappropriate for the purpose of this report. Daniewicz *et. al.* [13] presented expressions to determine the decreased tooth stiffness of a gear with a cracked tooth which further dictates fatigue resistance and gear noise. In the paper written by Umezawa *et. al.* [14], seven stiffness functions were discussed and it can be seen that even healthy gears exhibit the behaviours of variation of meshing stiffness.

First, a meshing stiffness for a pair of healthy gears is proposed to investigate the steady state response of meshing gears, two time-frequency distributions mentioned before are applied to monitor the conditions of gear teeth. The magnitude of the secondary force required to cancel the gear vibration is calculated, and the steady state response of this meshing gears with the secondary force applied are shown.

Following the results for healthy gears, the results of a pair of meshing gears with one defect on one tooth, which causes the decrease of meshing stiffness, are then presented.

Finally, the reason why the stiffness function suggested by Dalpiaz and Meneghetti is inappropriate for the purpose of this report is given.

For all results shown in figures (6.1 - 6.3), the governing equation (2.10) is integrated using the Runge-Kutta 4th order method to obtain the accelerations. Parameters set as follow unless specifically described: mass m=12 kg, damping c is set for a constant damping ratio $\zeta = 0.03$, primary force F=500 N, 512 samples in one rotation, the rotational speed of the gear is 600 RPM, N=16.

6.1 Healthy gears

Simulation results for a healthy gear are first shown to verify the results obtained in previous sections.

Figure (6.1a)

The meshing stiffness is set as: $k_0 = 5 \cdot 10^8 \, N/m$, $\alpha = 0.2$, i.e. $k = k_0(1 + \alpha \cos N\theta)$. Figure (6.1a) shows the meshing stiffness both in time domain and frequency domain.

Figure (6.1b)

Acceleration of the linear oscillator in time domain and frequency domain.

Figure (6.1c)

Wigner-Ville distribution of the acceleration shown in figure (6.1b), the dominant frequency can be seen is the meshing frequency, i.e. 16 shaft orders.

Figure (6.1d)

Sliced Wigner trispectrum, the SWT enhances the distribution in the time-frequency domain.

Figure (6.1e)

The secondary force required to completely suppress the gear vibration, which can be determined either from the stiffness modulation index α or from the Fourier coefficient of the meshing frequency of the acceleration shown in figure (6.1b).

Figure (6.1f)

The acceleration with applied secondary force in time and frequency domain. It can be seen that the gear vibration is suppressed.

6.2 Cracked gears

Figure (6.2a)

The meshing stiffness of cracked gear is set as: $k_0 = 5 \cdot 10^8 \, N/m$, $\alpha = 0.1$. The cracked tooth locates approximately from 180^0 to 200^0.

Figure (6.2b)

The acceleration of the linear oscillator in time domain and frequency domain. This system's natural frequency (≈ 110 shaft orders) can be clearly seen in time domain and frequency domain which complicates the response of the system.

Figure (6.2c)

Wigner-Ville distribution of the acceleration shown in figure (6.2b), the position of the fault can be observed from this figure.

Figure (6.2d)

Sliced Wigner trispectrum of the acceleration shown in figure (6.2b) which again shows the position of the fault.

Figure (6.2e)

The secondary force required to completely suppress the gear vibration, which can be determined either from the stiffness modulation index α or from the Fourier coefficient of the meshing frequency of the acceleration shown in figure (6.2b).

Figure (6.2f)

The acceleration with applied secondary force in time and frequency domain. It can be seen that the gear vibration is suppressed except the vibration introduced by the defect.

6.3 A different stiffness function

Figure (6.3a)

The stiffness function proposed by Dalpiaz and Meneghetti.

Figure (6.3b)

Acceleration generated by the variation of the meshing stiffness shown in figure (6.3a).

The dominant frequency of the acceleration is the natural frequency of this linear oscillator with two clear sidebands amplitude modulation which are resulted from the tooth meshing frequency.

Since the dominant frequency is neither the tooth meshing frequency, nor its harmonics, which does not agree with the reported results, hence is considered inappropriate. The discontinuity of the first derivative of the meshing stiffness might be the cause which excites the system periodically.

6.4 A more general stiffness variation function

The stiffness variation function described above might be found too coarse. A more general stiffness variation function with one dc term and two sinusodal terms is used in this section to show its effects in determining the secondary force.

The stiffness variation function used for results shown in figure (6.4) is set with a mean value $k_0=5*10^8$ N/m, plus one sinusoidal function at the meshing frequency with $\alpha_1 = 0.2$, and one sinusoidal at twice of the meshing frequency with $\alpha_2 = 0.05$.

Figure (6.4a)
The meshing stiffness.

Figure (6.4b)
Acceleration of the linear oscillator in time domain and frequency domain.

Figure (6.4c)
The secondary force required to completely suppress the vibration. The force shown here is determined by two stiffness modulation indices α_1 and α_2.

Figure (6.4d)
The acceleration with the secondary force applied in the time and frequency domains.

7. Conclusion

The vibration generated by meshing (healthy) gears can be predicted by utilising the variation of teeth meshing stiffness. This approach is also valid when there is a defect on one tooth of one of the meshing gears, the defect results in the decrease of meshing stiffness.

The force required for actuators mounted on a gear to suppress the gear vibration can be determined either from the stiffness modulation index or from the Fourier coefficient of the meshing frequency of the vibration signal.

The WVD and WHOMS are two useful time-frequency distributions in identifying the positions and frequencies of generated vibration signals of defects on gears.

Although the secondary forces generated by actuators cannot completely suppress the gear vibration when there is a defect on the gear, it provides an alternative method to enhance the SNR (signal to noise ratio). Here, the transient signal generated by the defect is crucial for the purpose of condition monitoring.

Moreover, referring to the results shown in figure (6.4), it can be concluded that by applying the secondary force to the meshing gear, the variation of meshing stiffness can be determined if the rotational acceleration of the gear can be suppressed.

Reference

[1] M.H. Chen and M.J. Brennan, "A simple gear model for investigating the active control of gear vibration and condition monitoring by vibration analysis", *ISVR Technical Memorandum No. 810*, November 1996.

[2] G.W. Blankenship and R. Singh, "Analytical solution for modulation sidebands associated with a class of mechanical oscillators", *Journal of Sound and Vibration*, 1995, 179(1), 13-36.

[3] T.J. Sutton and S.J. Elliott, "Active attenuation of periodic vibration in nonlinear systems using an adaptive harmonic controller", *Transactions of the ASME - Journal of Vibration and Acoustics*, 1995, 117(3), 355-362.

[4] J.K. Hammond and P.R. White, "The analysis of non-stationary signals using time-frequency methods", *Journal of Sound and Vibration*, 1996, 190(3), 419-447.

[5] W.J. Staszewski, K. Worden and G.R. Tomlinson, "Time-frequency analysis in gearbox fault detection using the Wigner-Ville distribution and pattern recognition", *Mechanical Systems and Signal Processing*, 1997, 11(5), 673-692.

[6] J.R. Fonollosa and C.L. Nikias, "Wigner higher order moment spectra: definition, properties, communication and application to transient signal analysis", *IEEE Transactions on Signal Processing*, 1993, 41(1), 245-266.

[7] C.L. Nikias and A.P. Petropulu, "Higher-Order Spectra Analysis", PTR Prentice-Hall, Inc., 1993, Chapter 11.

[8] S.K. Lee and P.R. White, "Higher-order time-frequency analysis and its application to fault detection in rotating machinery", *Mechanical Systems and Signal Processing*, 1997, 11(4), 637-650.

[9] S.L. Harris, "Dynamic loads on the teeth of spur gears", *A general meeting aranged in conjunction with the applied Mechanics Group*, London, October 1957, 87-112.

[10] Y. Cai and T. Hayashi, "The linear approximated equation of vibration of a pair of spur gears (theory and experiment)", *Transactions of the ASME - Journal of Mechanical Design*, 1994, 116(2), 558-564.

[11] H.A. Gaberson, "Application of Choi-Willaims reduced interference time frequency distribution to machinery diagnostics", *Shock and Vibration*, 1995, 2(6), 437-444.

[12] G. Dalpiaz and U. Meneghetti, "Detection and modelling of fatigue cracks in gears", *Condition Monitoring - Proceedings of the 3rd International Conference*, Edited by J.R. McEwan, 1991, 73-82.

[13] S.R. Daniewicz and J.A. Collins and D.R. Houser, "The stress intensity factor and stiffness for a cracked spur gear tooth", *Transactions of the ASME - Journal of Mechanical Design*, 1994, 116(3), 697-700.

[14] K. Umezawa, T. Sato and J. Ishikawa, "Simulation on rotational vibration of spur gears", *Bulletin of JSME*, 1984, 27(223), 102-109.

Appendix A. Steady-state solution of the simplified gear model

The steady-state solution for the simplied gear model with an applied secondary force is derived. Since the angle modulation is not considered (i.e. $\beta = 0$) in this LTI model, the angle parameter $\theta(\tau)$ can be written as:

$$\theta(\tau) = \Lambda\tau \tag{A.1}$$

Soem of the equations in the main text are repeated here for reference:

$$\delta(\theta) = \Delta_s \cos(\theta + \phi_s) \tag{2.13}$$

$$\ddot{\xi} + 2\zeta\dot{\xi} + \{1 + \alpha\psi[\theta(\tau)]\}\xi(\tau) = \{1 + \alpha\psi[\theta(\tau)]\}\hat{\xi}[f, \theta(\tau)] \tag{2.15}$$

$$[1 + \alpha\cos(N\theta)]^{-1} = \sum_{n=0}^{\infty} a_n \cos(nN\theta) \tag{2.17}$$

$$\ddot{\xi} + 2\zeta\dot{\xi} + \xi(\tau) = \hat{\xi}[f, \theta(\tau)] \tag{2.19}$$

Combining equation (2.19) together with equations (2.13), (2.15) and (2.17) becomes:

$$\ddot{\xi}(\tau) + 2\zeta\dot{\xi}(\tau) + \xi(\tau) = \Delta_s \cos(\Lambda\tau + \phi_s) + f \cdot \sum_{n=0}^{\infty} \cos(nN\Lambda\tau) + \Delta f \sum_{n=0}^{\infty} \cos(nN\Lambda\tau)\cos(N\Lambda\tau) \tag{A.2}$$

Equation (A.2) can be solved by separating the right-hand-side into three terms and equation (A.2) becomes three linear differential equations:

$$\ddot{\xi}(\tau) + 2\zeta\dot{\xi}(\tau) + \xi(\tau) = \Delta_s \cos(\Lambda\tau + \phi_s) \tag{A.3}$$

$$\ddot{\xi}(\tau) + 2\zeta\dot{\xi}(\tau) + \xi(\tau) = f \cdot \sum_{n=0}^{\infty} \cos(nN\Lambda\tau) \tag{A.4}$$

$$\ddot{\xi}(\tau) + 2\zeta\dot{\xi}(\tau) + \xi(\tau) = \Delta f \cdot \sum_{n=0}^{\infty} \cos(nN\Lambda\tau)\cos(N\Lambda\tau) \tag{A.5}$$

Since

$$\cos(\gamma) = \left(e^{j\gamma} + e^{-j\gamma}\right)/2$$

$$\cos\theta_1 \cos\theta_2 = \left[\cos(\theta_1 + \theta_2) + \cos(\theta_1 - \theta_2)\right]/2 = \left(e^{j(\theta_1+\theta_2)} + e^{-j(\theta_1+\theta_2)} + e^{j(\theta_1-\theta_2)} + e^{-j(\theta_1-\theta_2)}\right)/4$$

the steady state solution for equation (A.5) can be written as: (solutions of equation (A.3) and (A.4) can be found in Appendix B of [1])

$$\xi_{ss3}(\tau) = c_1 e^{j((n+1)N\Lambda\tau)} + c_2 e^{-j((n+1)N\Lambda\tau)} + c_3 e^{j((n-1)N\Lambda\tau)} + c_4 e^{-j((n-1)N\Lambda\tau)} \tag{A.6}$$

Substituting equation (A.6) into equation (A.5), and collecting terms, coefficients c_1, c_2, c_3, and c_4 can be written as:

$$c_1 = \frac{a_n/4}{1-((n+1)N\Lambda)^2 + j2\zeta((n+1)N\Lambda)} \tag{A.7}$$

$$c_2 = \frac{a_n/4}{1-((n+1)N\Lambda)^2 - j2\zeta((n+1)N\Lambda)} \tag{A.8}$$

$$c_3 = \frac{a_n/4}{1-((n-1)N\Lambda)^2 + j2\zeta((n-1)N\Lambda)} \tag{A.9}$$

$$c_4 = \frac{a_n/4}{1-((n-1)N\Lambda)^2 - j2\zeta((n-1)N\Lambda)} \tag{A.10}$$

The steady state solution of equation (A.2) can be written as:

$$\xi_{ss}(\tau) = \xi_{ss1}(\tau) + \xi_{ss2}(\tau) + \xi_{ss3}(\tau) \tag{A.11}$$

where ξ_{ss1} contains the displacement excitation (Δ_s) terms, ξ_{ss2} the primary force (f) terms, and ξ_{ss3} the secondary force (Δf) terms. Equation (A.11) can be further written as:

$$\begin{aligned}
\xi_{ss}(\tau) &= \xi_{ss1}(\tau) + \xi_{ss2}(\tau) + c_1 e^{j((n+1)N\Lambda\tau)} + c_2 e^{-j((n+1)N\Lambda\tau)} + c_3 e^{j((n-1)N\Lambda\tau)} + c_4 e^{-j((n-1)N\Lambda\tau)} \\
&= \frac{\Delta_s\left[(1-\Lambda^2)\cos(\Lambda\tau+\phi_s) + (2\zeta\Lambda)\sin(\Lambda\tau+\phi_s)\right]}{(1-\Lambda^2)^2 + (2\zeta\Lambda)^2} \\
&\quad + f\cdot\sum_{n=0}^{\infty} \frac{a_n\left\{\left[1-(nN\Lambda)^2\right]\cos(nN\Lambda\tau) + 2\zeta(nN\Lambda)\sin(nN\Lambda\tau)\right\}}{\left[1-(nN\Lambda)^2\right]^2 + \left[2\zeta(nN\Lambda)\right]^2} \\
&\quad + \Delta f\cdot a_0 \frac{\left\{\left[1-(N\Lambda)^2\right]\cos(N\Lambda\tau) + 2\zeta(N\Lambda)\sin(N\Lambda\tau)\right\}}{\left[1-(N\Lambda)^2\right]^2 + \left[2\zeta(N\Lambda)\right]^2} \\
&\quad + \Delta f\cdot\sum_{n=1}^{\infty} \frac{a_n}{2} \frac{\left\{\left[1-((n+1)N\Lambda)^2\right]\cos((n+1)N\Lambda\tau) + 2\zeta((n+1)N\Lambda)\sin((n+1)N\Lambda\tau)\right\}}{\left[1-((n+1)N\Lambda)^2\right]^2 + \left[2\zeta((n+1)N\Lambda)\right]^2}
\end{aligned}$$

$$+\Delta f \cdot \sum_{n=1}^{\infty} \frac{a_n}{2} \frac{\left\{\left[1-\left((n-1)N\Lambda\right)^2\right]\cos\left((n-1)N\Lambda\tau\right)+2\zeta\left((n-1)N\Lambda\right)\sin\left((n-1)N\Lambda\tau\right)\right\}}{\left[1-\left((n-1)N\Lambda\right)^2\right]^2+\left[2\zeta\left((n-1)N\Lambda\right)\right]^2} \tag{A.12}$$

This concludes the derivation of the steady-state solution of the simplified gear model.

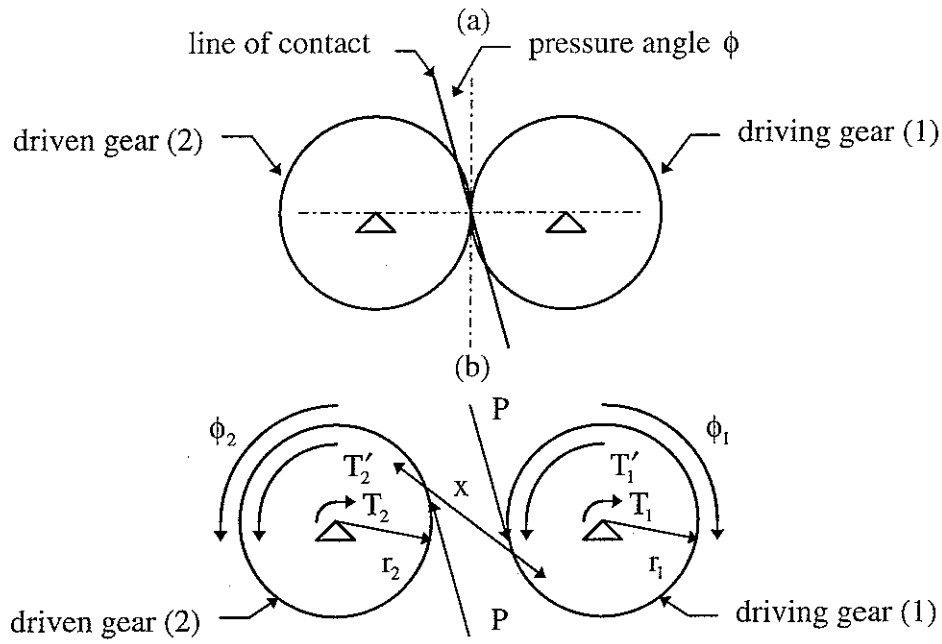

Figure (2.1) (a) A pair of meshing gears, (b) free body diagram of meshing gears.

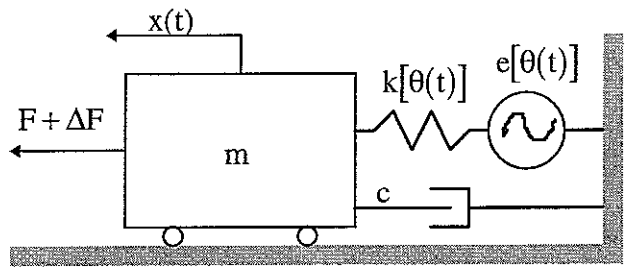

Figure (2.2) The physical system: a single DOF system with spatially periodic stiffness $k[\theta(t)]$ and displacement excitation $e[\theta(t)]$ under a mean applied force F and a time-varying applied force ΔF.

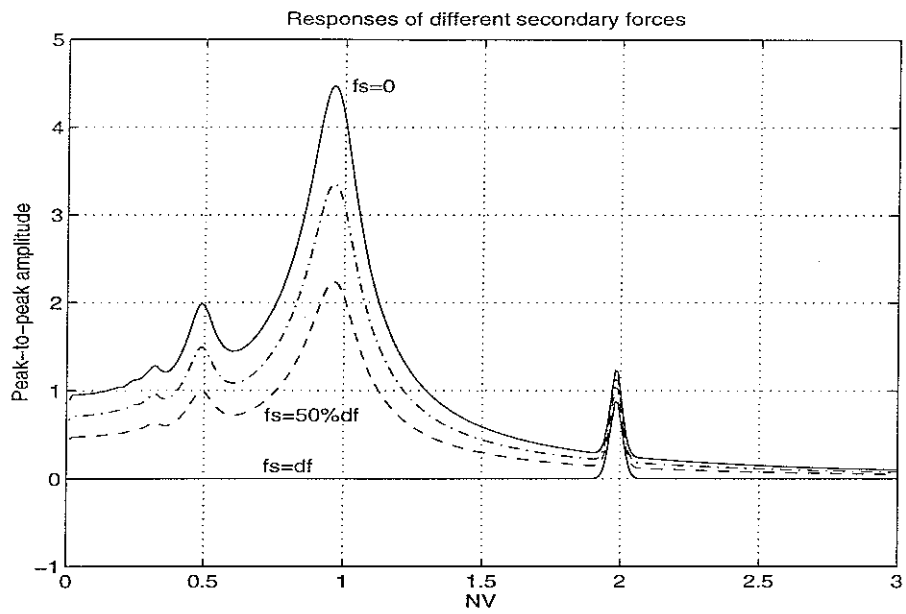

Figure (2.3) Peak-to-peak amplitude of steady state responses ξ_{ss}/f with different secondary forces, ·····, $f_s = 0.25\Delta f$.

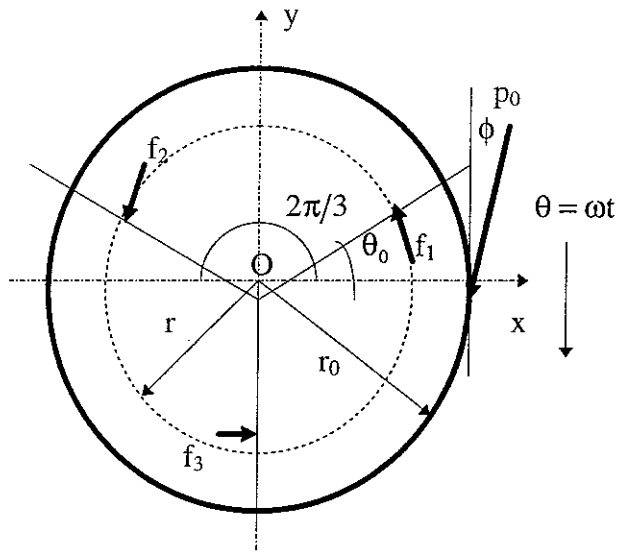

Figure (3.1) Configurations of three actuators on a gear.

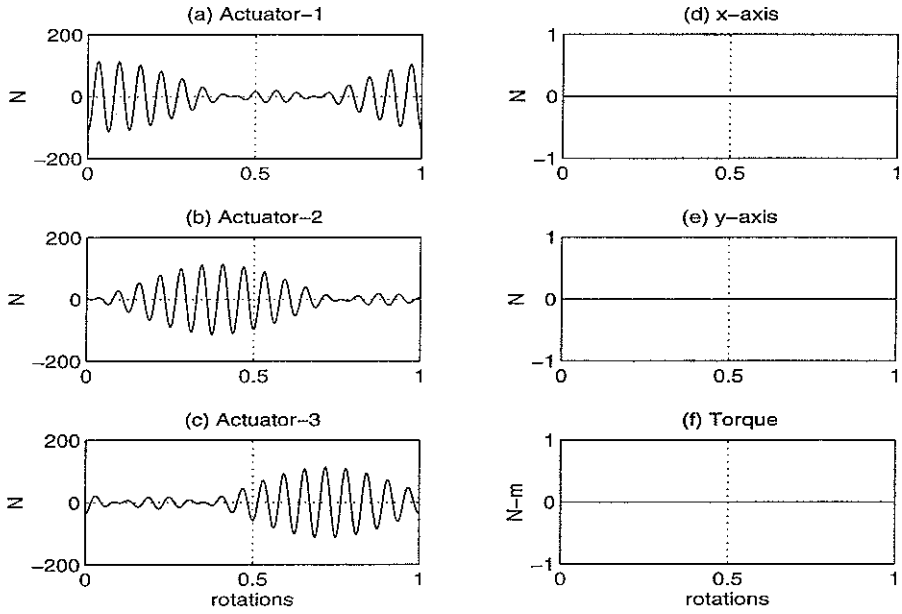

Figure (3.2) Forces required for actuators to cancel gear vibration.

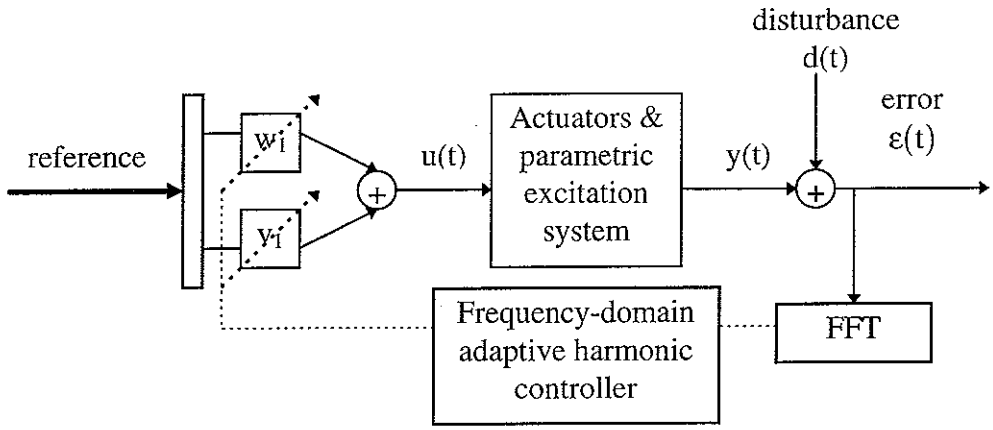

Figure (4.1) Block diagram of the adaptive harmonic controller.

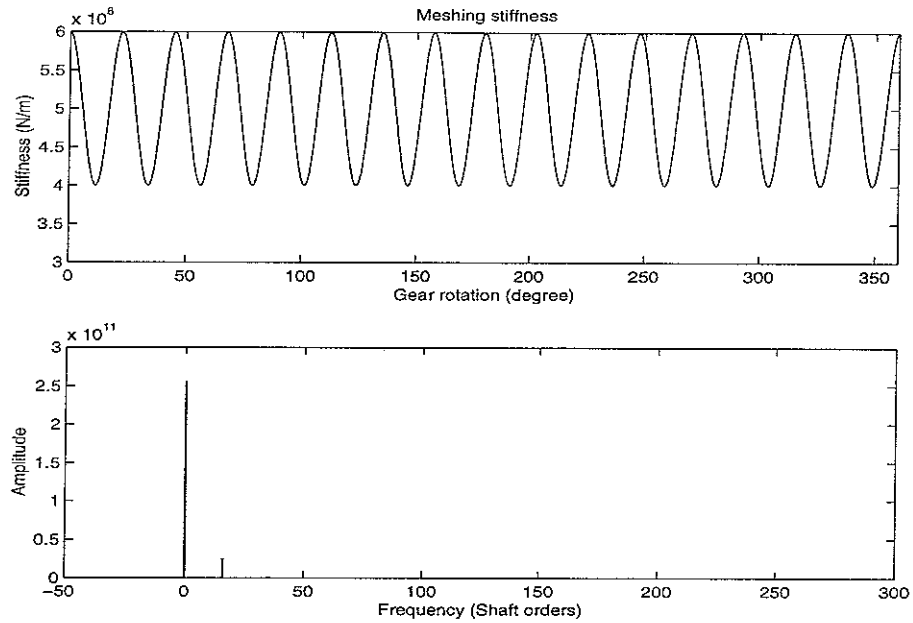

Figure (6.1a) Meshing stiffness and its Fourier transform.

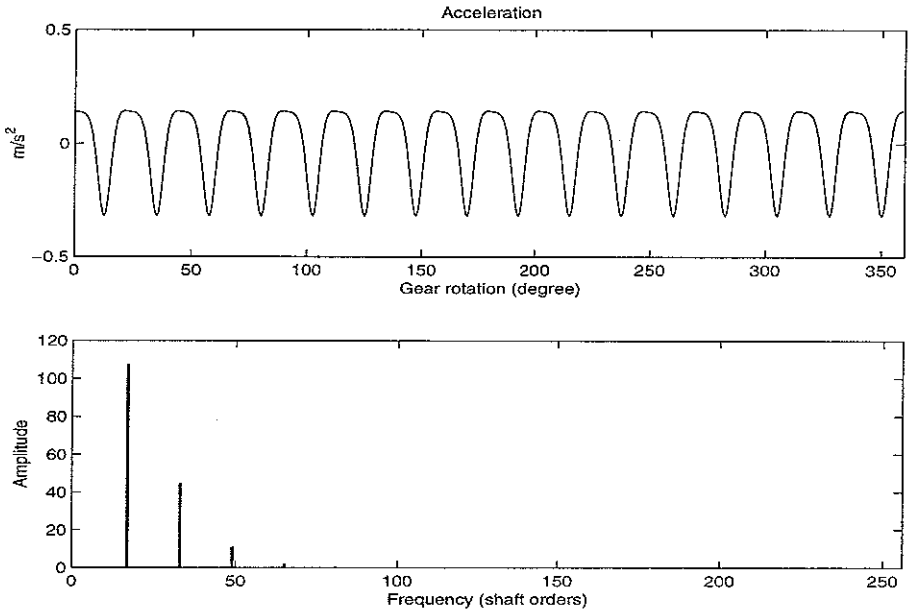

Figure (6.1b) Measured acceleration and its Fourier transform.

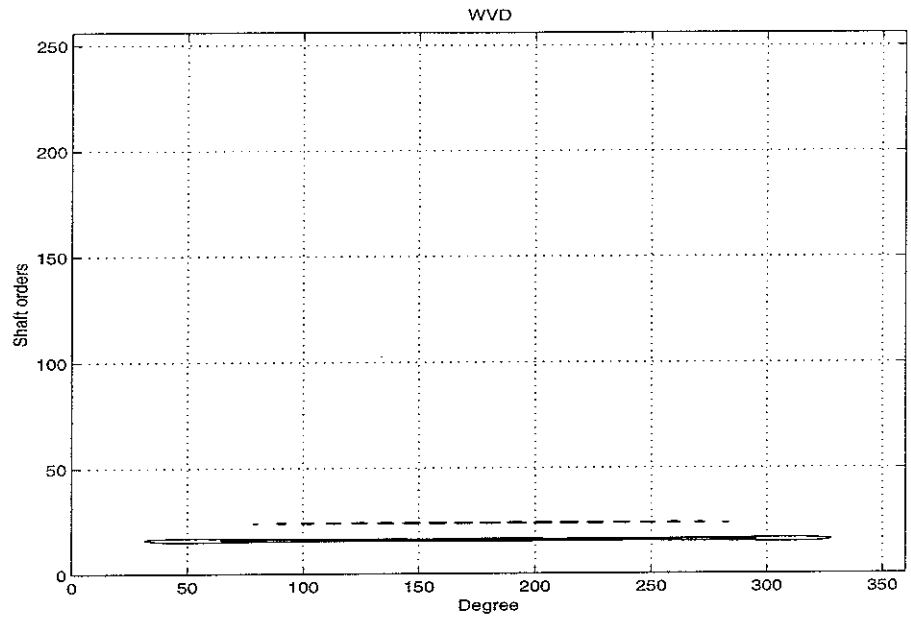

Figure (6.1c) Wigner-Ville distribution of the acceleration.

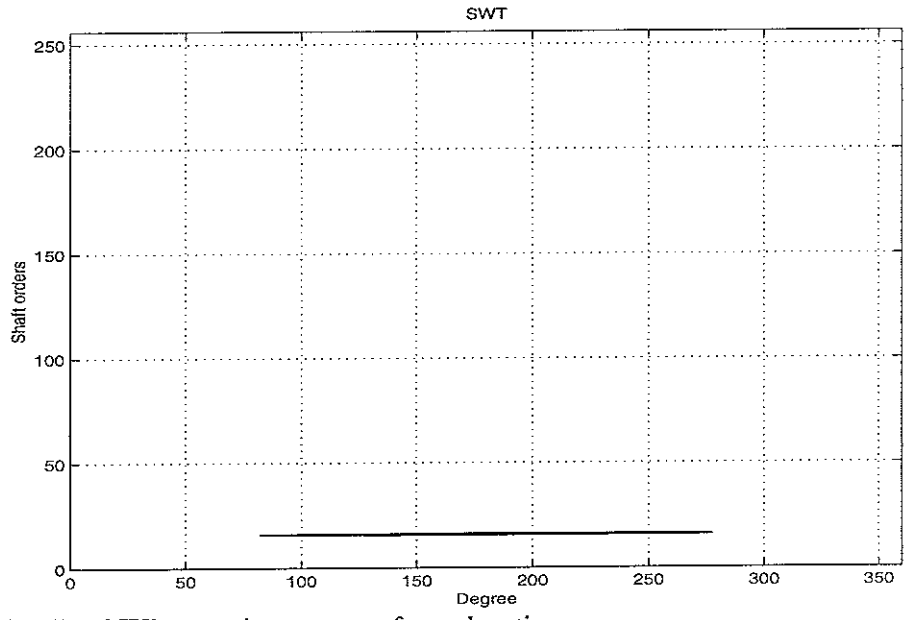

Figure (6.1d) Sliced Wigner trispectrum of acceleration.

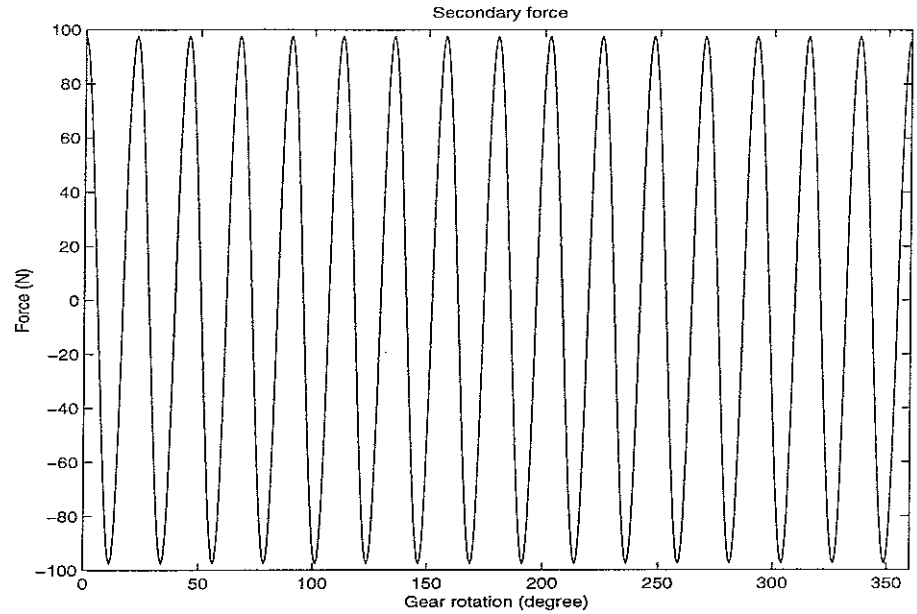

Figure (6.1e) Waveform of the output of the harmonic controller.

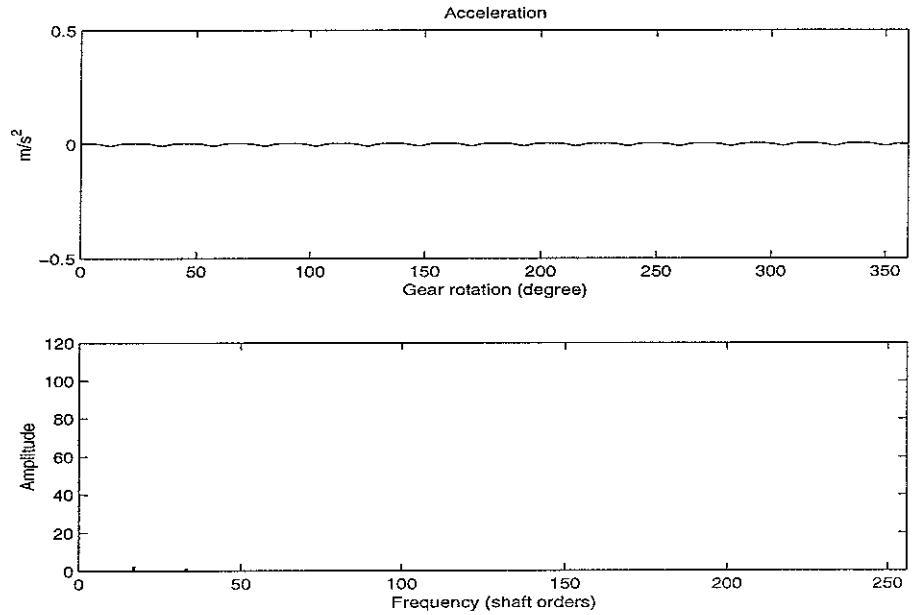

Figure (6.1f) Acceleration with the secondary force.

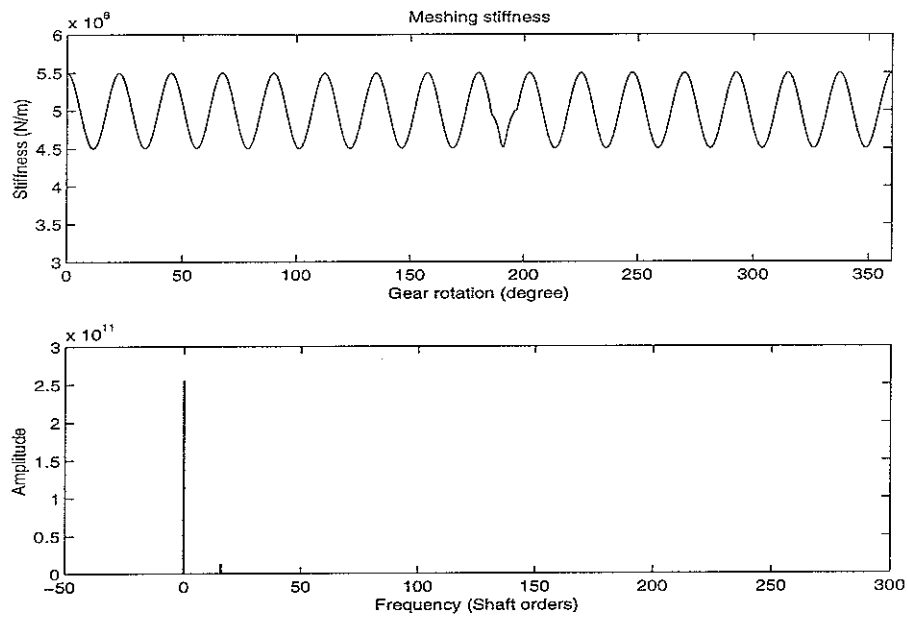

Figure (6.2a) Meshing stiffness and its Fourier transform.

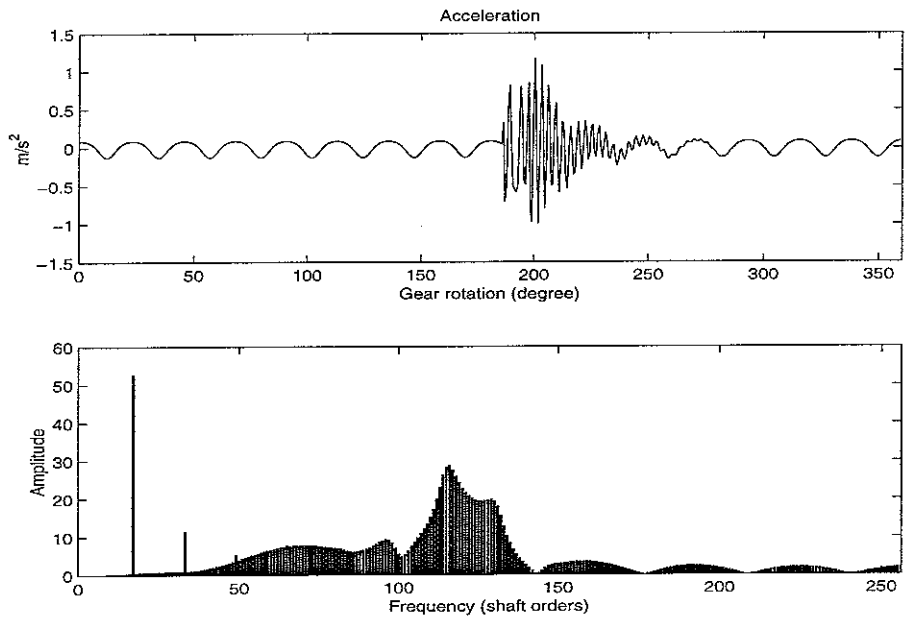

Figure (6.2b) Acceleration and its Fourier transform.

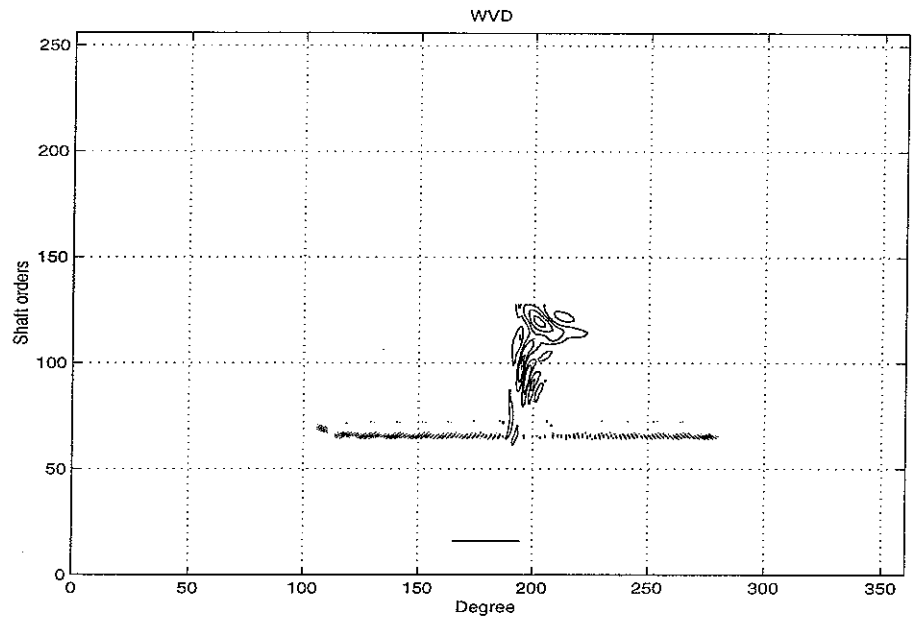

Figure (6.2c) Wigner-Ville distribution of acceleration.

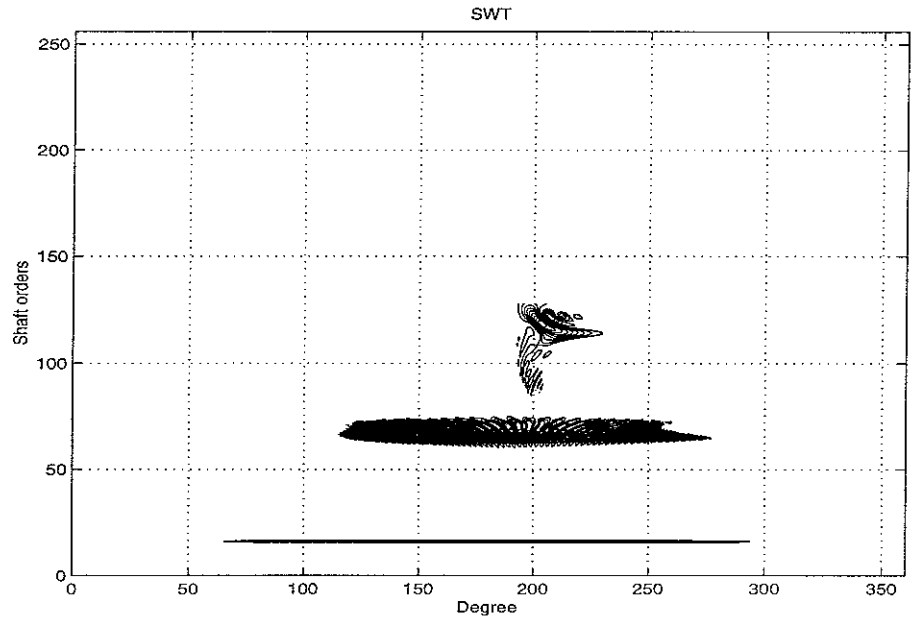

Figure (6.2d) Sliced Wigner trispectrum of acceleration.

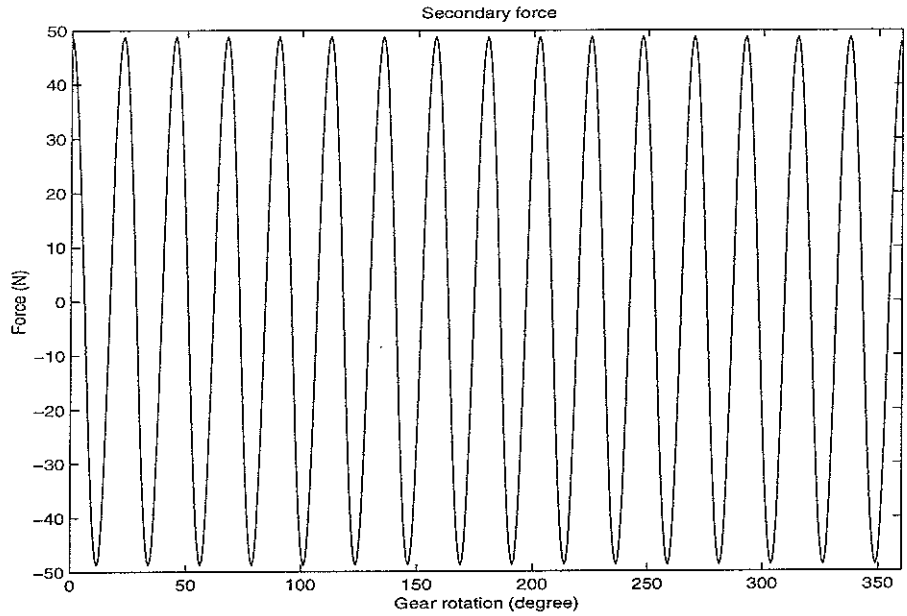

Figure (6.2e) Waveform of the output of the harmonic controller.

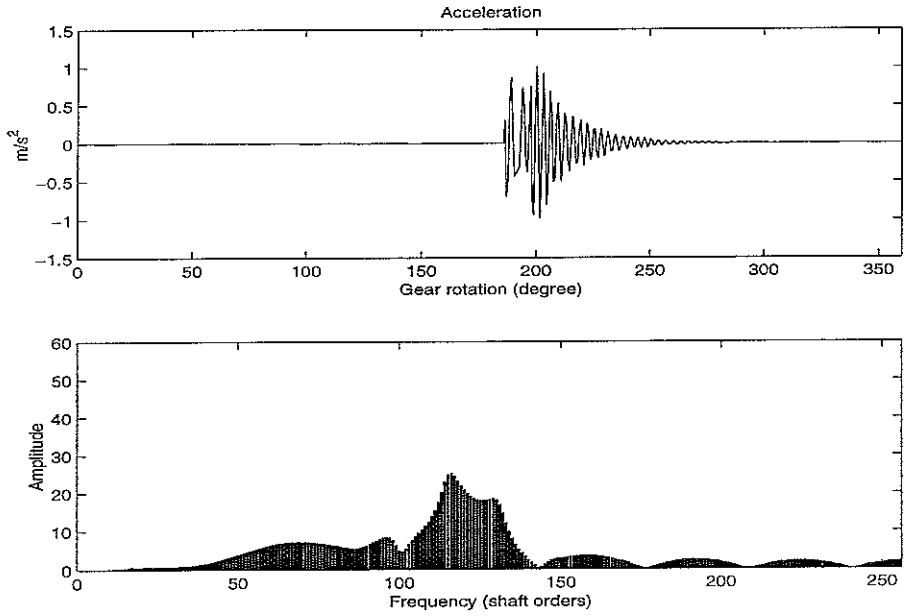

Figure (6.2f) Acceleration with the secondary force.

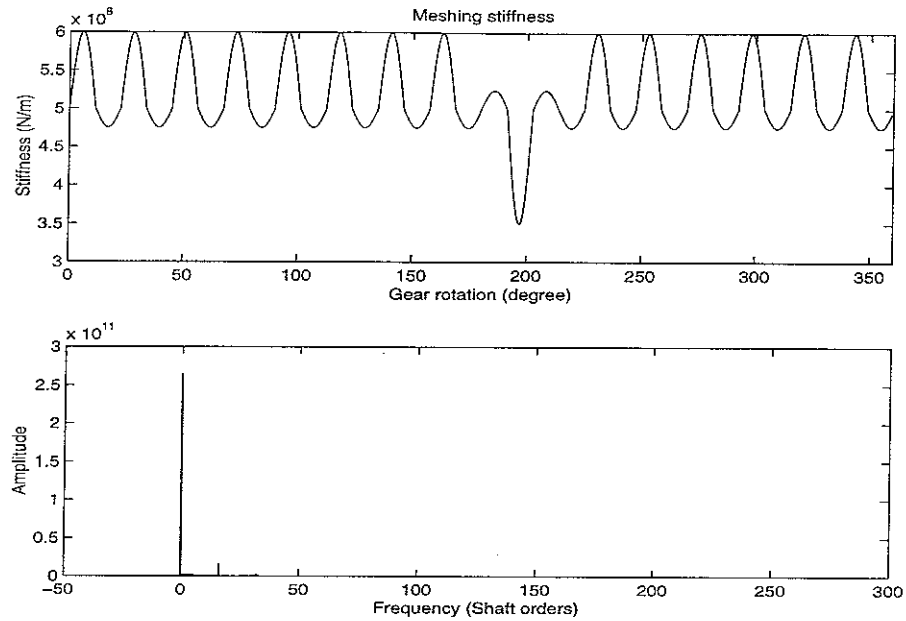

Figure (6.3a) Meshing stiffness and its Fourier transform.

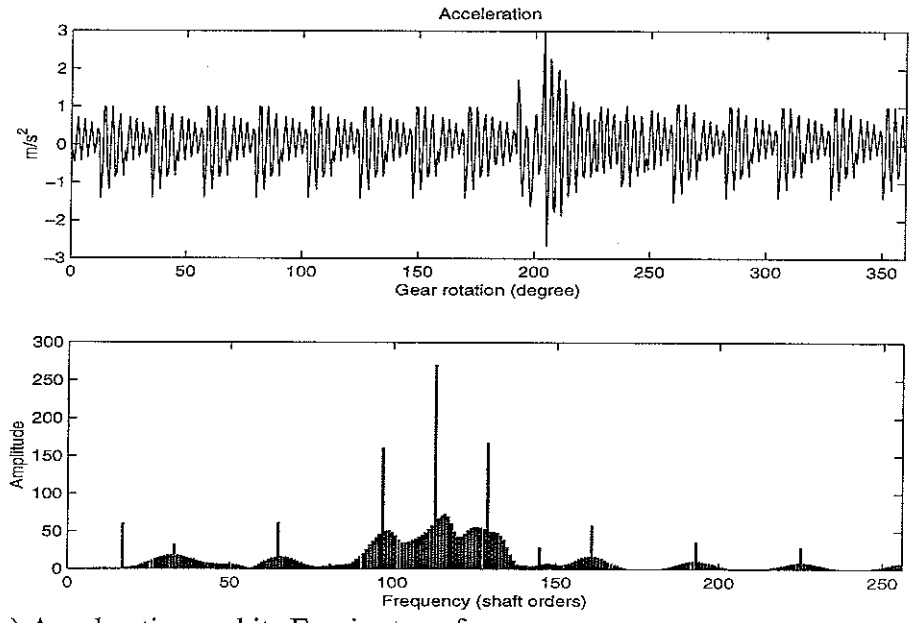

Figure (6.3b) Acceleration and its Fourier transform.

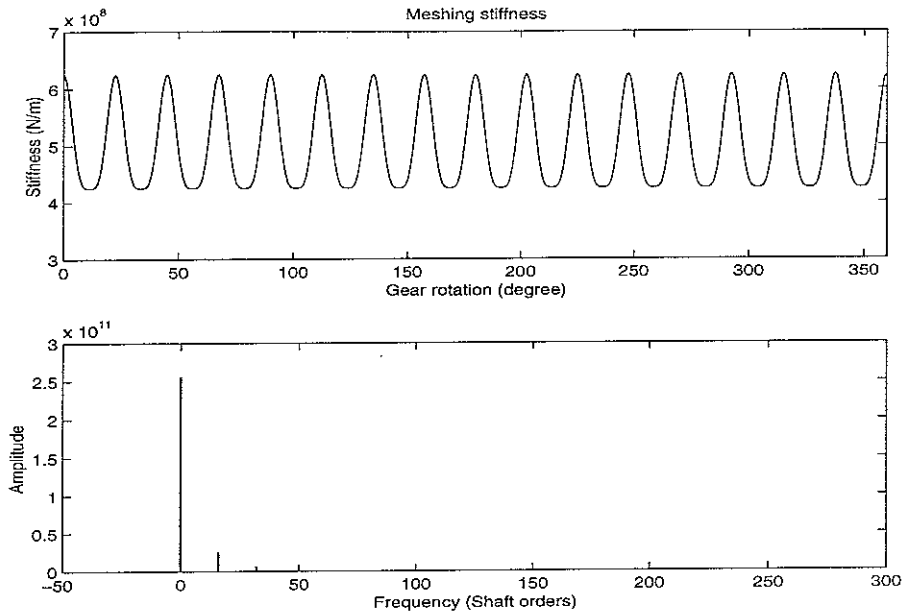

Figure (6.4a) Meshing stiffness and its Fourier transform.

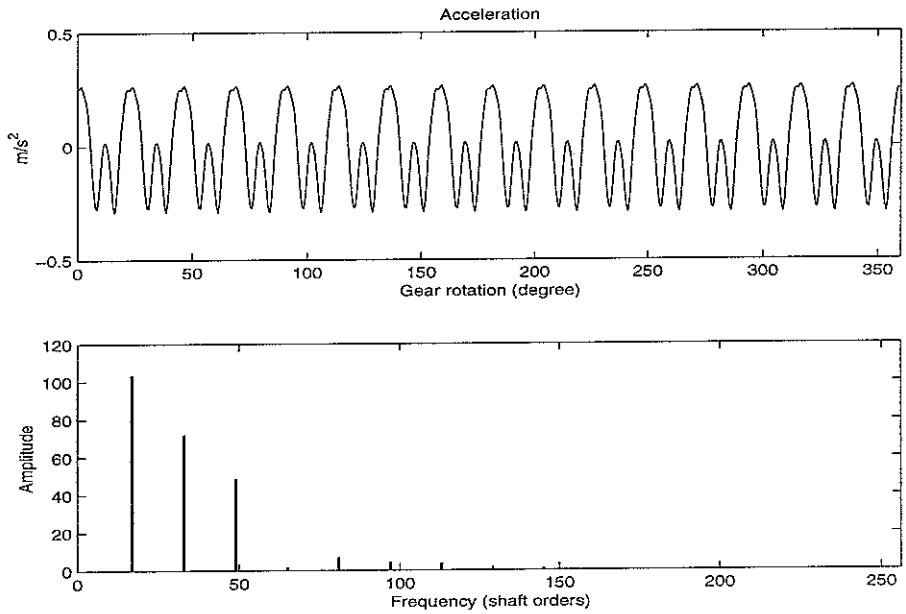

Figure (6.4b) Measured acceleration and its Fourier transform.

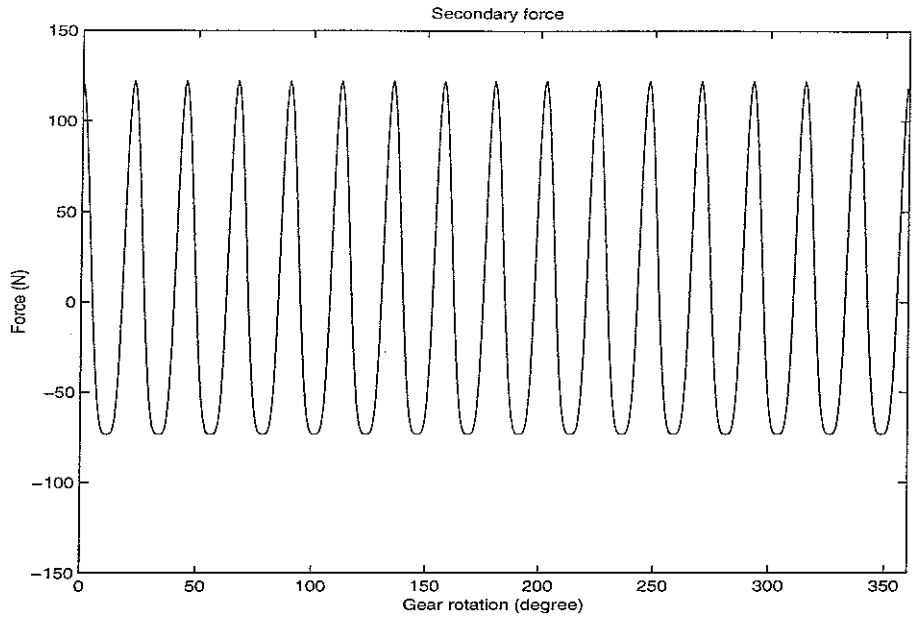

Figure (6.4c) Waveform of the output of the harmonic controller.

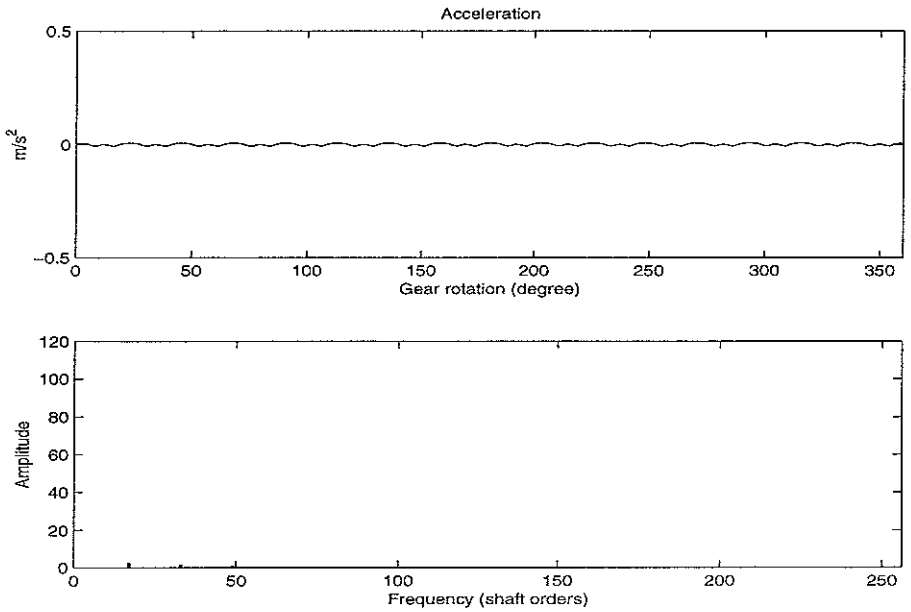

Figure (6.4d) Acceleration with the secondary force.